based on the flow velocity in the vertical leg. This loss is shown on Fig. 2 by starting the p-u curve for the flow entering the vertical leg from zero velocity instead of from the actual velocity that exists and constructing the curve to show a loss of one-half the dynamic head. The losses specified in this way are consistent with the two limiting cases of no flow into the vertical leg, where static pressure should exist, and flow from zero velocity in the straight tube, where the loss based on the inflow dynamic head is taken because of the poor inlet configuration.

The solutions can now be carried out by assuming different shock strengths and then using the continuity relation at the T juncture to determine the relative area ratios appropriate to the conditions assumed. If a particular area ratio is desired, different conditions can be assumed until the required area ratio is obtained. The conditions shown correspond to equal areas in all legs of the T.

Calculations for a T configuration with equal area legs have been made for various shock strengths and the losses as assumed previously (Fig. 3). Compared with experimental measurements made in the reference, the agreement is reasonable for both subsonic and supersonic cases. Other values of the loss coefficients, particularly higher values of the loss coefficient based on the inflow dynamic head for the supersonic cases, would give better results. Measurement of these losses by steady-state experiments would be useful. For initial shock strengths that give Mach numbers near 1 ($P_s \sim$ 56 psi), no solution is possible using the loss coefficients selected, indicating that they are not correct for these Mach numbers. The extension of this model to L junctures and other configurations is obvious and will not be considered here.

One use of this model is to correlate the experimental data, such as in Ref. 1, in terms of a few loss coefficients and to provide a tool for extrapolating to other values of initial shock strength. Its more important use is to provide a boundary condition at the juncture to use in unsteady flow calculations by the method of characteristics. Empirical data will probably never be available to provide the detailed information of what happens as waves of different types (such as multiple reflections due to the downstream configuration of the two legs) impinge upon the T and some analytic model such as this one is required to provide a self consistent boundary condition.

Reference

[1] "Information summary of blast patterns in tunnels and chambers," Ballistic Research Labs. Memo. Rept. 1390, 2nd ed. Defense Atomic Support Agency Rept. 1273 (March 1962).

Model Law for Parachute Opening Shock

KENNETH E. FRENCH*
Lockheed Missiles and Space Company, Sunnyvale, Calif.

Nomenclature

C_D = drag coefficient, dimensionless
D_0 = canopy constructed diameter, ft
F = net force on system, lb
F_p = peak opening shock, lb
f_j = functional relationship (j = 1, 2)
g = acceleration of gravity, ft/sec^2
k = coefficient of proportionality, dimensionless
l_s = parachute suspension-line length, ft
M = mass of chute plus mass of attached load, slug

Received July 20, 1964.
* Research Specialist. Member AIAA.

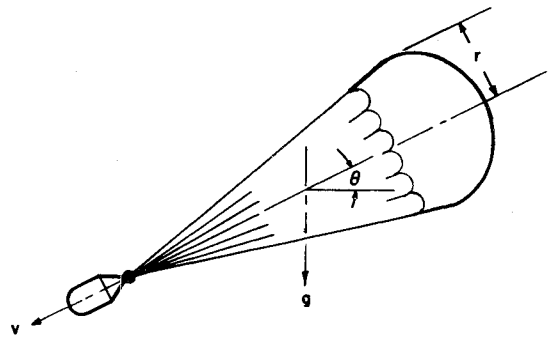

Fig. 1 Diagram of system.

m_{air} = mass of air within and associated with inflating chute, slug
q = instantaneous dynamic pressure, lb/ft^2
q_0 = dynamic pressure at beginning of inflation, lb/ft^2
R = maximum projected radius of fully inflated chute, ft
r = instantaneous value for chute maximum projected radius, ft
r_0 = chute maximum projected radius at beginning of inflation, ft
S = πr^2 = chute reference drag area, ft^2
S_0 = $\pi D_0^2/4$ = chute reference drag area based on canopy cloth area, ft^2
v = instantaneous value of velocity, fps
v_0 = velocity at beginning of inflation, fps
θ = angle of inclination to the horizontal, deg or rad
π = a pure number = 3.14...
ρ = atmospheric mass density, slug/ft^3

Introduction

PARACHUTE opening shock, the maximum force developed during inflation of a parachute, has been the subject of several theoretical investigations (for additional references on opening shock see Ref. 1, pp. 272–274). Of these, Pounder's excellent work[2] appears to provide the most rational and thorough analysis. In view of the date of Pounder's work (1956), it is somewhat surprising that no model law for parachute opening shock is currently regarded as acceptable.[3] The lack of application of Pounder's work is apparently due to its mathematical complexity and its requirement for rather good test data on the inflation sequence for a particular type of parachute. Because of these obstacles to rapid, practical application of Pounder's theory, it is desirable to develop simple, approximate scaling laws for parachute opening shock. Such a development and its correlation with test data are the subjects of this paper.

Dimensional Analysis

Consider the problem of dynamical similarity in determining peak opening shock in the testing of a parachute. For simplicity, assume that the parachute inflates along a flight path of constant inclination and that the suspended load has

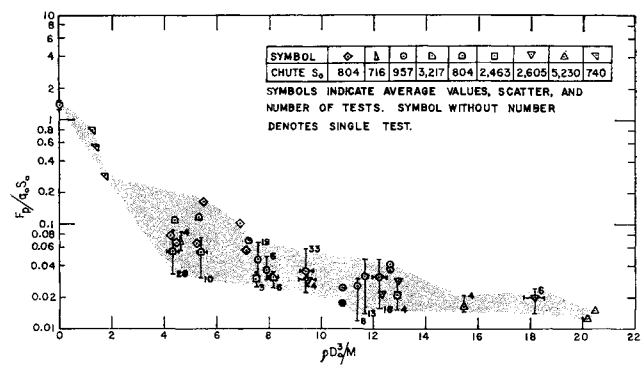

Fig. 2 Euler number vs mass ratio.

Table 1 Summary of data on extended skirt-type parachutes[a]

Parachute configuration				Range of test parameters[b]						
Skirt extension, %	S_0, ft²	l_s/D_0	N/D_0,[c] ft⁻¹	Mg/S_0, lb/ft²	v_0, fps	q_0, lb/ft²	Reynolds number, $\times 10^{-6}$	Mach number	Froude number	Number of tests
10.0	804	1.00	0.63	0.67	262	79	52	0.23	67	6
				0.42	193	42	38	0.17	36	
10.0	716	0.75	0.93	0.23	150	25	280	0.13	24	4
10.0	957	0.73	0.86	0.23	504	190	86	0.47	227	102
					185	25	31	0.17	30	
10.0	3217	0.74	0.53	0.73	231	59	89	0.20	26	6
				0.49	194	43	77	0.17	18	
12.5	804	1.00	0.75	0.71	337	127	66	0.29	110	40
			0.50	0.54	196	44	30	0.17	37	
12.5	2463	0.70	0.57	0.68	263	76	93	0.23	38	7
				0.39	228	57	80	0.20	29	
12.5	2605	0.71	0.94	0.64	336	147	119	0.32	61	12
				0.33	224	63	79	0.21	26	
14.3	5230	0.99	1.00	0.48	447	226	223	0.39	77	6
				0.35	279	87	138	0.24	30	
15.0	452	1.00	0.67	0.28	240	14	10	0.25	74	3
					180	6	5	0.19	42	

[a] Data from Ref. 5, except: data for 15% extended skirt ($S_0 = 452$) parachute from Ref. 6, and data for $\rho D_0^3/M = 0$ in Fig. 2 from Ref. 1.
[b] Where two numbers are given, the top denotes maximum and the bottom denotes minimum.
[c] N is the number of gores in parachute canopy.

negligible drag area relative to that of the inflating chute. With the use of these assumptions and for the system shown in Fig. 1, the force-balance equation is

$$F = mg \sin\theta - \tfrac{1}{2}\rho v^2 C_D \pi r^2 \quad (1)$$

where

$$m = \text{total mass of system} = M + m_{\text{air}} \quad (2)$$

Following the custom of dimensional analysis,[4] assume that the volume of air within, and associated with, the canopy may be taken as proportional to a characteristic canopy dimension cubed. This assumption gives

$$m_{\text{air}} = k\rho r^3 \quad (3)$$

And, hence

$$m = M + k\rho r^3 \quad (4)$$

Substituting Eq. (4) back into Eq. (1) and rearranging,

$$(\pi/2)\{(\rho r^3/M)/[1 + (k\rho r^3/M)]\}(1/\tfrac{1}{2}\rho v^2)(1/\pi r^2)F = (\sin\theta gr/v^2) - (C_D\pi/2) \times \{(\rho r^3/M)/[1 + (k\rho r^3/M)]\} \quad (5)$$

In Eq. (5), $\frac{1}{2}\rho v^2$ is the instantaneous dynamic pressure, πr^2 is the instantaneous canopy reference area, and k and C_D are characteristic of a given class or type of parachute.† For a given type or class of parachute, Eq. (5) therefore may be written in the form

$$F/qS = f_1[(gr \sin\theta/v^2), (\rho r^3/M)] \quad (6)$$

Or, replacing the variable radius r with the constructed canopy diameter D_0, the variable velocity v with the velocity at beginning of inflation v_0, and the variable net force F with the peak opening shock F_p:

$$F_p/q_0S_0 = f_2[(gD_0 \sin\theta/v_0^2), (\rho D_0^3/M)] \quad (7)$$

which is the required model law. Note that, in Eq. (7), F_p/q_0S_0 and $gD_0 \sin\theta/v_0^2$ are variants of the Euler and Froude numbers,[4] respectively, whereas $\rho D_0^3/M$ is a dimensionless "mass ratio" resulting from the analysis.

† As discussed later, C_D may also be a function of the Reynolds number.

Test Data

If the relationship shown in Eq. (7) is valid, it should be possible to plot F_p/q_0S_0 vs $\rho D_0^3/M$ (or $gD_0 \sin\theta/v_0^2$) at $gD_0 \sin\theta/v_0^2 = \text{const}$ (or at $\rho D_0^3/M = \text{const}$) for geometrically similar parachutes and thus to determine the nature of the function f_2. Unfortunately, however, available parachute test data are too limited both in range and adequate reporting of test conditions to permit a comprehensive coverage of the independent variables. This writer, therefore, has taken data available on extended skirt-type parachutes[1, 5, 6] and plotted Euler number vs mass ratio in Fig. 2 without any consideration of the Froude-number-related variable $gD_0 \sin\theta/v_0^2$. Details on parachute configurations and the range of test variables covered by the data of Fig. 2 are shown in Table 1.

Figure 2, which covers slightly more than two decades of Euler numbers, is surprisingly well correlated in view of the facts that one of the independent variables ($gD_0 \sin\theta/v_0^2$) has been neglected and that the test data are for parachutes that, though generally similar, differ in important details (e.g., N/D_0 ratio). The data must also be viewed in the knowledge that even repeated tests of the same parachute system under the same release conditions show standard deviations in F_p/q_0S_0 values of up to $\pm 26\%$.[7]

In an effort to determine the significance of the $gD_0 \sin\theta/v_0^2$ parameter, Euler number has been plotted vs Froude number at about constant mass ratio in Fig. 3 for the only parachute configuration with sufficient test data available to do this. Figure 3 shows that the test data spread of Fig. 2 is further reduced by taking into account Froude-number variations.

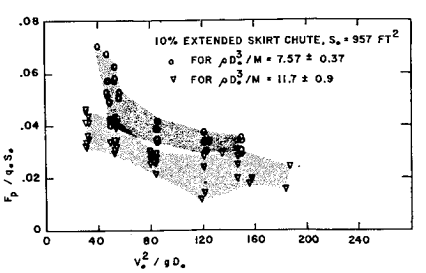

Fig. 3 Euler number vs Froude number at constant mass ratio.

Discussion

Considering that Figs. 2 and 3 are based primarily on test data that give launch speed rather than v_0‡ and that offer no clue as to variations of the angle θ in the Froude-number-related parameter $gD_0 \sin\theta/v_0^2$, the data of the figures are sufficiently well correlated to indicate the general validity of the model law set forth in Eq. (7).

Since the test data used (cf. Table 1) are for cases well below Mach 1, compressibility effects do not enter into any of the scatter observed in Figs. 2 and 3. However, in the derivation of Eq. (7) it was assumed that C_D could be treated solely as a characteristic of the parachute, which may not be the case. That is, although the relatively high Reynolds numbers of Table 1 appear to justify neglect of viscous effects, the Reynolds numbers of the table are based on parachute diameter D_0, which does not appear to be the best choice of a characteristic length for flow of air through the canopy. A better choice would be a Reynolds number based on some characteristic dimension of the canopy material, and the resulting (lower) Reynolds numbers might well be significant with respect to opening shock.

Equation (7) indicates that both $\rho D_0^3/M$ and $gD_0 \sin\theta/v_0^2$ must be held constant for dynamical similarity in free-flight testing of parachute opening shock. It is, in fact, physically possible to maintain simultaneously both of these parameters at their correct values. The model law and data presented herein also indicate that proper adjustment of the test variables may be used to test opening shock at low altitude on a parachute system intended for use at high altitude, to extrapolate opening shock test data on scale models to full scale, and to test in the earth's atmosphere parachute systems intended for use in other planetary atmospheres. However, it is obvious that more and better test data are required to verify completely any model law for incompressible flow parachute opening shock, with data particularly required at $\rho D_0^3/M$ numbers from 0 to, say, 5.

References

[1] "Performance of and design criteria for deployable aerodynamic decelerators," Aeronautical Systems Div., ASD-TR-61-579, Wright-Patterson Air Force Base, pp. 149–164, 272–274 (December 1963).

[2] Pounder, E., "Parachute inflation process wind tunnel study," Wright Air Development Center, TR 56-391, Wright-Patterson Air Force Base (September 1956).

[3] Shepardson, W. P., "Progress in aerodynamic decelerator research and development," Proceedings of Retardation and Recovery Symposium, Tech. Doc. Rept. Aeronautical Systems Div. ASD-TDR-63-239, Wright-Patterson Air Force Base, pp. 6–12 (May 1963).

[4] Bennett, C. O. and Myers, J. E., *Momentum, Heat, and Mass Transfer* (McGraw-Hill Book Co., Inc., New York, 1962), Chap. 14, pp. 147–163.

[5] Walcott, W. B., "Study of parachute scale effects," Tech. Doc. Rept. Aeronautical Systems Div., ASD-TDR-62-1023, Wright-Patterson Air Force Base, pp. 57–62 (January 1963).

[6] "Discoverer parachute improvement program," Lockheed Missiles and Space Co., Rept. LMSD-447720 (January 20, 1961).

[7] Heinrich, H. G. and Scipio, L. A., "Performance characteristics of extended skirt parachutes," Wright Air Development Center TR 59-562, Wright-Patterson Air Force Base (October 1959).

‡ It is difficult to obtain a value for v_0 corresponding to a definite radius r_0 for the chute in an early stage of inflation, whereas it is a trivial matter to report the airspeed at which a packed parachute is launched from an aircraft or test vehicle. The result is, unfortunately, that only the launch speed is usually reported.

Capillary Stability in an Inverted Rectangular Channel for Free Surfaces with Curvature of Changing Sign

PAUL CONCUS*

University of California, Berkeley, Calif.

Nomenclature

B = Bond number
F = equilibrium interface
x, y = nondimensional Cartesian coordinates
Δ = $\pm$ curvature
ϵ = variational parameter
η = perturbation to F
θ = contact angle
λ = undetermined parameter
ψ = angle between tangent to F and horizontal
$(\ )'$ = differentiation with respect to x

Introduction

IN a previous paper,[1] an investigation of the stability of an incompressible inviscid fluid contained in an inverted rectangular channel was performed mathematically with the effects of surface tension taken into account. The purpose was to determine the effect of contact angle and Bond number on the stability of such a fluid configuration in a low-gravity environment. The investigation was restricted to those fluid-gas equilibrium interfaces for which the curvature does not change sign. The analysis is extended in this report to include equilibrium interfaces for which the curvature does change sign. The omission of such interfaces in the original analysis is shown to be justified because they are all dynamically unstable. In addition, the details omitted in Ref. 1 of the calculation of the critical Bond number for equilibrium interfaces for which the curvature does not change sign are also presented.

Formulation

The differential equation for an equilibrium free surface $y = F(x)$ (see Fig. 1) is given by Eq. (3) of Ref. 1 as

$$\{F'/[(1 + F'^2)]^{1/2}\}' + BF - \lambda = 0 \qquad -1 < x < 1 \quad (1)$$

The boundary conditions are given by Eq. (4) of Ref. 1 and are

$$F'(1) = -F'(-1) = \cot\theta \quad (2)$$

where θ is the contact angle between the fluid and the wall. Only values of θ for which $0 < \theta < \pi/2$ (wetting fluid) will be considered, since, as was shown in Ref. 1, the problem for $\pi/2 < \theta < \pi$ (nonwetting fluid) can be formulated in terms of an equivalent problem for $0 < \theta < \pi/2$.

Equation (1) can be solved in terms of the parameter

$$\psi = \tan^{-1}F' \quad (2a)$$

the slope of the surface, to yield

$$B(F^2/2) - \lambda F = \cos\psi - C$$

where F is now a function of ψ. The boundary conditions, Eq. (2), become $\psi = \pm(\pi/2 - \theta)$ at $x = \pm 1$, respectively. The constant of integration C may be conveniently evaluated by choosing the origin of coordinates properly. The coordinates shown in Fig. 1 of Ref. 1 were chosen so that the origin would lie on the fluid-vapor interface, halfway between the walls. It is more convenient here to choose the x axis to

Received July 21, 1964. This work was carried out mainly under the Independent Research Program of the Lockheed Missiles and Space Company and secondarily under the auspices of the U. S. Atomic Energy Commission.

* Mathematician, Lawrence Radiation Laboratory.